TASK QUARTERLY 6 No 1 (2002), 25–37

NUMERICAL SIMULATION OF THE INFLUENCE OF A FILLET AND A BULB ON THE SECONDARY FLOW IN A COMPRESSOR CASCADE

MARTIN HOEGER[1], UWE SCHMIDT-EISENLOHR[1], SOPHIE GOMEZ[2], HELMUT SAUER[3] AND RALF MÜLLER[3]

[1] *MTU Aero Engines, Dachauer Straße 665, 80995 München, Germany*
martin.hoeger@muc.mtu.de

[2] *University of Valenciennes, UVHC BP 311, 59304 Valenciennes Cedex, France*
Sophie_Gomez@gmx.de

[3] *Dresden University of Technology, Institute of Fluidmechanics, D-01062 Dresden, Germany*
Ralf.Mueller2@mailbox.tu-dresden.de

(Received 15 August 2001)

Abstract: Large fillet radii are typically found on highly loaded compressor rotors to ensure structural integrity. The objective of this paper is to investigate the impact of such real geometry effects on the flow at the hub section. Investigations were performed numerically for the idealised case of a plane compressor cascade with the 3D Navier-Stokes code TRACE_S. Realistic inlet boundary layer displacement thickness and typical loading levels close to stall are considered at low inlet Mach numbers $\mathrm{Ma}_1 = 0.23$.

A large fillet with a relative radius of 16% chord length is considered as well as a 3D leading edge bulb-configuration designed at TU Dresden. The results are discussed in terms of iso-Mach surfaces, secondary flow patterns and spanwise incidence and turning. A complex 3D vortex system rises from the fillet radius, which improves the aerodynamic behaviour of the cascade at the end-wall section. With the bulb configuration the suction surface horse-shoe vortex leg was demonstrated to weaken the undesirable cross flow and by that to reduce the hazard of corner stall.

Keywords: secondary flow, compressor cascade, fillet, bulb

1. Introduction

In the past years axial compressor development has shown a continuing tendency towards highly loaded low aspect ratio designs (wide chord design), with the aim to minimise blade counts as well as engine and maintenance costs. It is pointed out

by Denton [1] that such low aspect ratio blading in combination with high turning results in a fully three dimensional flow field for which to control endwall flows is critically important.

Conventional rotor blades are manufactured with minimum fillet radii at the junction of blade and hub platforms. For advanced designs with high tip speeds the rotors are fabricated as blisk designs, *i.e.* blades and disk are made of one single piece. For blisk rotors large fillet radii are applied to ensure mechanical integrity. In a similar way large fillet radii are applied for struts and cast stator vanes, where stress peaks in the corner between vane and annulus must be avoided. In the latter cases fillet radii can have a size which amounts to a substantial fraction of the passage width. Since the fillet is also apparent at the leading and the trailing edge, it is obvious that it must have an impact on the development of secondary flow and discharge flow angle.

One possibility in looking on the fillet influence is the less stable 3D boundary-layer developing in a corner from the interference of the blade- and the endwall viscous flow. As studied by Debruge [2] the addition of a fillet for a compressor blade will result in a thinner boundary layer in the corner region that is less likely to separate. For a Double Circular Airfoil, DCA, Curlett [3] demonstrated that fillets do not significantly change losses at low to moderate incidence angles. However, as the incidence angle was increased, the cascades with finite fillet radii were found to have measurably lower losses. Calvert and Ginder [4] are in line with this result mentioning that large fillet radii may be applied for aerodynamic reasons. In contradiction to the findings for the DCA-profile, Curlett [3] and Breugelmans [5] found increased secondary flow and higher losses for a Controlled Diffusion Airfoil, CDA, when adding a fillet. The results clearly indicate that for this configuration fillet size should be kept as small as possible. A similarly situated real geometry effect is reported by Escuret *et al.* [6]: a mismatch in radial position for the variable stator vane buttons resulted in a 1% efficiency drop and increased corner stall. In this paper an attempt is made to show the influence of the fillet on the secondary flow for a plane compressor cascade.

2. Background and motivation

As pointed out by LeJambre *et al.* [7] 3D Navier-Stokes based design systems allow a reduction in cost by about 50% and an improvement in efficiency of up to 2%. Precondition is that all relevant parameters like *e.g.* fillets, cavities and unsteady mixing are captured, which are approximately included in an integral manner by semi-empirical formula in traditional compressor design systems. To optimise real geometry configurations and create an experimental basis for code validation, blade shapes with modified thickness at the hub are studied for a linear compressor cascade. In a cascade the flow phenomena are elaborated more precisely without being influenced by 3D effects. As part of national AG Turbo II programme, cascade design and numerical investigation are performed at MTU Aero Engines. Experiments are conducted at the TU Dresden low speed cascade wind tunnel. First results obtained for the reference blade confirm the theoretical findings given in this paper.

3. Cascade design

3.1. Aerodynamic design

The cascade design is similar in velocity distribution and boundary layer behaviour to a rotor endwall section of the 4-stage Low Speed Compressor Rig Dresden, LSCD, see Boos *et al.* [8], which itself consists of a CDA-type airfoils comparable to modern compressor designs. Cascade mid section Q3D Mach number distributions are given in Figure 1. In the present paper the flow close to stalled operation with 7° incidence is discussed. In the vicinity of the endwall the datum design shows a beginning corner stall with a boundary layer separation on the suction surface. Here average values for DeHaller number and diffusion factor are 0.55 and 0.6, respectively.

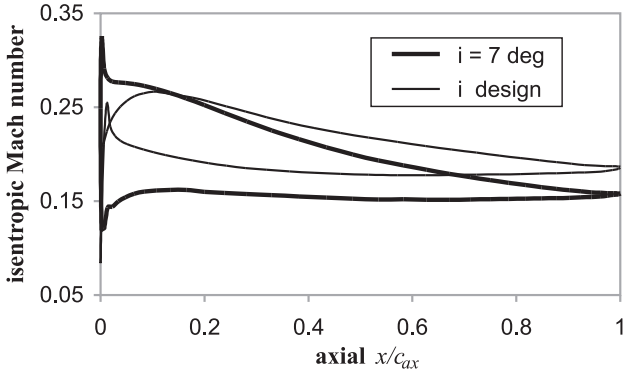

Figure 1. Cascade midsection isentropic Mach number distributions at design and 7° incidence (present investigation)

3.2. Relevance of cascade approach

With no rotation and no endwall contraction for the incompressible flow in cascade a different stream tube geometry is obtained compared to the one found in a compressor. Together with the requirement of similarity in velocity distribution and profile boundary layer behaviour this results in a different airfoil geometry with reduced turning. Although the Mach number level as such is thought not to dominate secondary flows, the missing of rotation and blade interaction effects, like *e.g.* a spanwise non-uniformity in inlet flow angle, prevents a direct application of the present results to compressor flows. In an actual compressor the inlet skew of the endwall boundary layer profile changes the secondary flow pattern. In addition for a rotating blade separating boundary layer material is centrifuged towards the tip.

The 2D cascade represents the special case of a vane with uniform inlet flow angle and a radius ratio close to unity and is as such thought to enable relevant flow investigations, see Roberts *et al.* [9] for typical compressor vane flow angle behaviour. The better understanding gained from the cascade experiment then may be transformed into improved designs by adding all further 3D effects found in an actual compressor component.

3.3. Cascade geometry

The geometric and aerodynamic parameters of the cascade are given below, a representation of the cascade is found in Figure 2: chord length, $c = 0.100\,\mathrm{m}$; pitch-chord ratio, $p/c = 0.62$; relative maximum thickness, $t/c = 5.5\%$; aspect ratio $H/c = 3.0$; turning $\Delta\beta = 21.5^{\circ}$; incidence relative to design conditions $i = 7^{\circ}$; inlet Mach number $\mathrm{Ma}_1 = 0.23$; inlet boundary layer displacement thickness, $\delta^*/c = 2.5\%$ chord; Reynolds number, $\mathrm{Re}_c = 5.1 \cdot 10^5$.

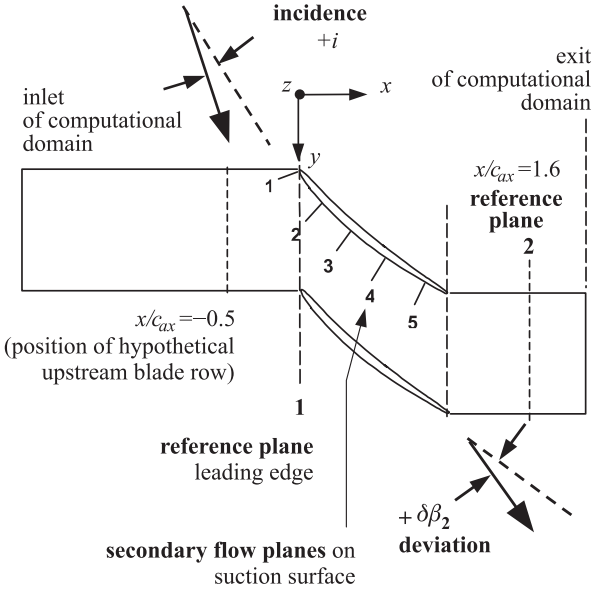

Figure 2. Cascade geometry, reference planes and flow angle definitions

3.4. Modified thickness distribution

Fillet Radius The fillet is constructed in a conventional way, but slightly modified at the endwall. Here the fillet surface intersects the hub under an angle of about 25° to ease grid generation by standard tools, see Figure 3 (bottom) for an H/O-grid surface close to the endwall-fillet junction and Figure 3 (top) for a view of the fillet geometry in the meridional plane. Actually the angle between the fillet surface and the hub region approaches values close to zero yielding diamond-shaped mesh cells which may cause numerical inaccuracies and lower the stability of the code, see Turner *et al.* [10]. In Figure 4 (top) a pitch-wise view of the cascade blade with a relative fillet radius of 16% chord is given together with a cross section close to mid chord. Considerable blockage is generated by the fillet. In addition some results of an 8% chord fillet configuration are presented.

Bulb Geometry The bulb geometry was developed at TU Dresden and was successfully used to improve secondary flow in turbine cascades, see Sauer *et al.* [11]. For a pitch-wise and cross sectional view of the blade with bulb, see Figure 4 (bottom). The profile sections used to build up the blade shape are indicated by straight lines, see pitchwise view in Figure 4 (left). The empirically given bulb shape shown in Figure 5 is

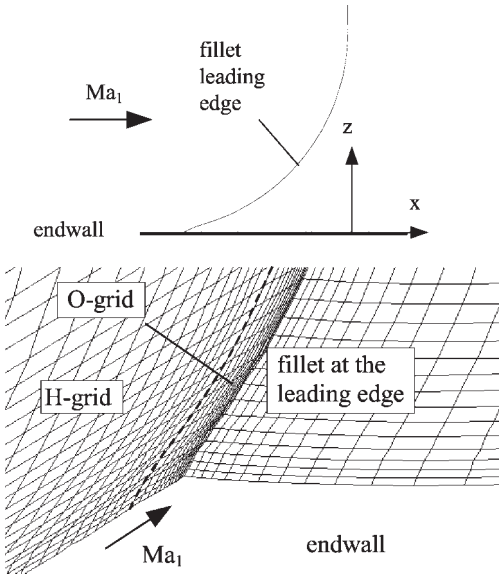

Figure 3. Fillet geometry at the hub (top) and grid detail at the fillet-endwall junction (bottom)

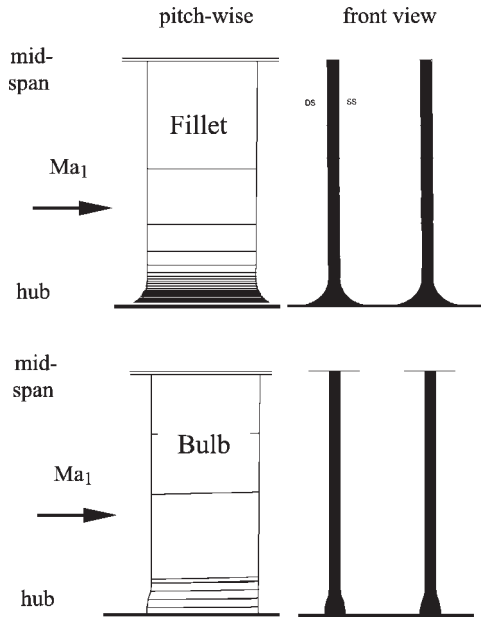

Figure 4. Reference blade with 16% R/c fillet (top) and bulb configuration (bottom)

kept constant over a height b_0 and approaches the reference profile over an increasing wall distance by a cosine function, see spanwise bulb thickness distribution in Figure 6.

4. Numerical simulations

4.1. 3D Navier Stokes

Details of the Navier-Stokes solver TRACE_S, an explicit cell-centered 2^{nd}-order-accurate finite-volume scheme, are given in Fritsch *et al.* [12]. Grid Topology and

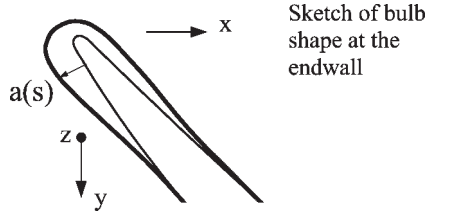

Figure 5. Empirically given bulb thickness distribution $a(s)$ at the leading edge (surface length s)

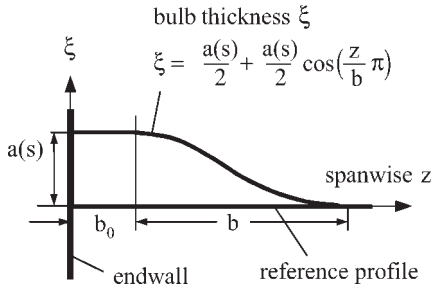

Figure 6. Bulb thickness variation ξ in spanwise direction z

CPU-Time: All simulations utilized a composite H/O-grid, see Figure 7, with 165×41 nodes for the H-grid and 169×13 nodes for the O-grid in the S1-plane of the blade. From symmetry considerations only one half of the passage is considered. With 65 points in spanwise direction a total of 670 462 nodes was used. Extensive grid studies, partly documented in Fritsch *et al.* [13], were performed to ensure that (for the basic phenomena addressed here) the results of the simulations are not compromised by a lack of resolution. Execution time to convergence is approximately 28 CPU-hours on an SGI-Power Challenge computer using a single R-8K processor.

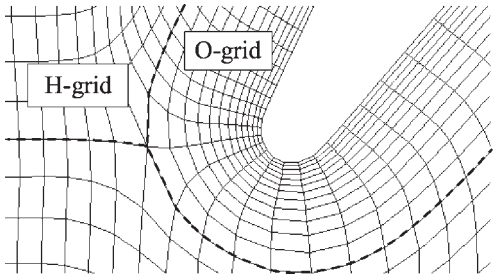

Figure 7. O/H-grid combination at the mid section

Turbulence Model: For economy a high Reynolds' k-ε model, resulting in a mean wall distance of $y+ = 25$ for the blade and $y+ = 10$ to 30 for the hub, was used.

All simulations were run fully turbulent with wall functions applied to accurately represent the wall shear. A turbulence level of 4% was used at the inlet. Additional predictions (not given here) were performed with a more sophisticated low Reynolds turbulence model, which yielded somewhat stronger secondary flows but underlined the present findings in principle.

4.2. Kutta condition

The build-up of circulation for an aerodynamic device was demonstrated by Kutta and Jukowsky to be dependent on the so-called Kutta-condition: Provided the trailing edge is thin compared to the chord length, a smooth exit flow is obtained with no singular jump in pressure across the trailing edge. For the present investigations with large fillet radius three characteristic zones may be distinguished in spanwise direction:

1. the blade itself which obeys the Kutta-condition,
2. a transition zone where the fillet creates a large trailing edge thickness and
3. the fillet body close to the endwall, which may be regarded simply as a 3D displacement body which as such creates neither circulation nor flow turning.

While flows at (1) and (3) are subject to steady flow simulations, the transition zone (2) shows blunt body character. Although it covers only a small fraction of the blade height, it should be kept in mind that unsteady phenomena are likely to rise there, which can be predicted precisely only by unsteady methods.

4.3. Evaluation of results

Pre- and post-processing were performed with in-house tools, flow visualisation with VISUAL and TECPLOT.

Reference Conditions Reference planes, see Figure 2, are the exit plane of a hypothetical upstream blade row at $x/c_{ax} = -0.5$, the cascade inlet plane and a downstream station at $x/c_{ax} = 1.6$. With changes in nose geometry from the bulb and the fillet, the leading edge is situated at different axial locations.

Averaging Conservative variables from the momentum equations are used to obtain pitch-averaged flow quantities.

Secondary flow definition The definition of secondary flow chosen here is linked to the orientation of the reference planes normal to the endwall and normal to the suction surface as given in Figure 2 (note: plane position for individual configurations may vary slightly). With the 2D (main) flow defined close to the suction surface all deviations from the direction tangent to the surface and tangent to the endwall are interpreted as secondary flow. The definition has the advantage of resolving vortex-like flows close to the blade, like *e.g.* from the interference of the suction surface and the endwall boundary layer, see Debruge [2]. On the other hand it has the disadvantage that any departure from flow direction with increasing distance from the suction surface will be interpreted as secondary flow.

5. Analysis of results

The discussion of the results is performed on the basis of classical secondary flow physics. Among many authors contributing to physical understanding of secondary flows the reader is referred to the basic work of: Hawthorne [14], and Came and Marsh [15] for secondary flow theory, Langston [16] for endwall flow topology and Sieverding [17] for a survey on the subject.

5.1. Endwall flow

Due to the reduced speeds in the boundary layer the flow at the endwall is no longer balanced with the static pressure imposed by the main flow. The pressure gradient drives the flow in pitchwise direction across the passage towards the suction surface forming the so-called passage vortex, see Figure 8. Flow regions with fluid originating from the inlet flow area are separated by a separation line SL from downstream regions. The separation line is linked with the horse-shoe vortex and forms a saddle point SP, where it intersects with the attachment line. Only low Mach numbers are found at the endwall close to the suction surface trailing edge but there is no fully

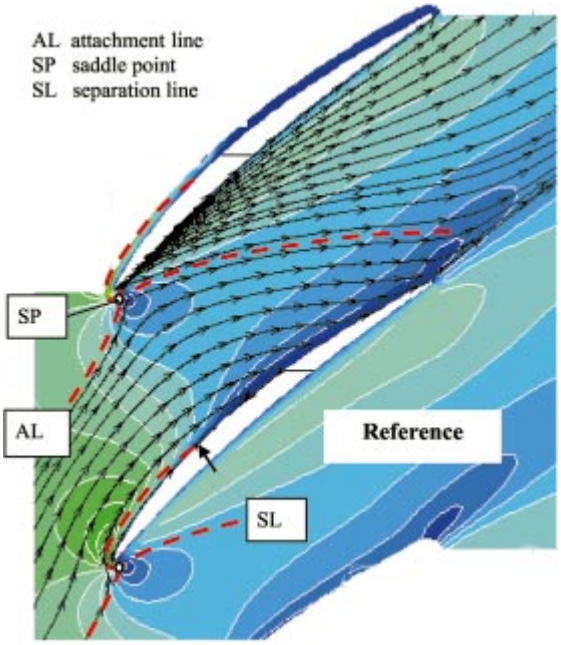

Figure 8. Streamlines and Iso-Mach contours at 1st grid node at the endwall

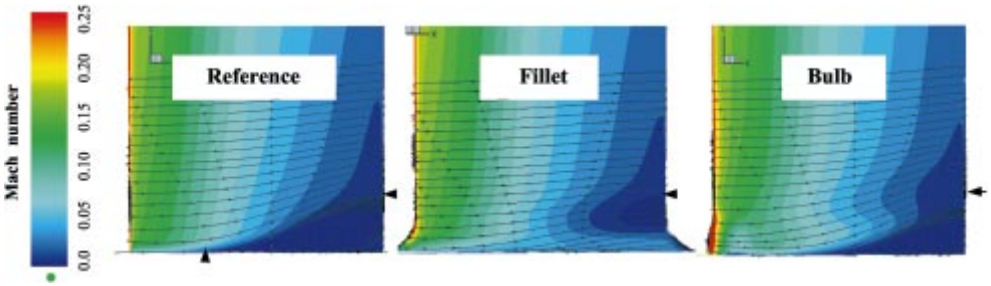

Figure 9. Streamlines and Iso-Mach surfaces on 1st grid nodes at the suction surface

developed corner stall with a second saddle point visible in Figure 8; for flow structure at stalled operation, see Stark and Bross [18].

5.2. Streamlines on suction surface

In Figure 9 streamlines on the suction surface in the 1st nodes of the O-grid are compared for the three configurations together with the Iso-Mach contours. The most striking feature is a large separation present for the reference blade, which is reduced in size by the bulb configuration, Figure 9 (right side), and completely removed for the blade with fillet radius, Figure 9 (mid). The span-wise extension of the separation zone for the reference case (as obtained by the intersection of the 3D separation limiting line with the trailing edge) is indicated by an arrow in Figure 9. A characteristic relative maximum in Mach number for the bulb and the fillet configuration may be attributed to the transport of high energy fluid to the suction surface close to the endwall, see following chapter.

5.3. Secondary flow patterns

To shed light on the flow mechanisms involved in the reduction of suction side separation shown in Figure 9, the secondary flow patterns are investigated in 5 planes normal to the suction surface in Figure 10; for plane position see Figure 2. To facilitate the interpretation of secondary flow movements, vortex-like flow structures are indicated by large arrows in a qualitative manner.

Reference Case When starting the flow visualisation, some effort was spent to trace the roll up of the horse-shoe vortex in front of the leading edge, but only a downwash of streamlines was found, see the reference blade in Figure 10, plane 1. Between plane 1 and 2 a suction surface horse-shoe vortex leg clearly was detected to build up. This vortex pattern reduced in size rapidly and only a small fraction of the vortex is found in plane 2. The roll up of the passage vortex is observed already ahead of the throat, where only a weak pressure gradient from suction surface overspeeds acts on the endwall flow, see Figure 10, plane 3. This observation may be explained by the theoretical model of Came and Marsh [15]. Under the influence of the suction side acceleration the inlet boundary layer is skewed and a vorticity component in axial direction is generated. This so-called distributed vorticity supports the roll up of the passage vortex. In a similar way the generation of the suction side horse-shoe vortex leg may be attributed to the bulge of the inlet boundary layer vortex filament line in the suction surface nose region. The roll up and decay of a suction surface leg of the horse-shoe vortex was observed in a similar way for a 2° incidence case not presented here. Downstream of the throat the passage vortex transports low energy material towards the suction surface leading to a complex 3D separation, see plane 4 and 5.

Bulb Configuration With the bulb configuration, the suction surface horse-shoe vortex leg is strengthened by the increased leading edge thickness, see Figure 10 (right side) planes 1 and 2. Driven by a beneficial radial pressure gradient generated in the rear part of the bulb, high momentum fluid on the suction surface travels downwards to the endwall. Velocities counteracting the passage vortex are induced and the convective loss transport to the suction surface is weakened, see plane 4 and 5 in Figure 10 (right side).

Fillet Radius Similar to the bulb configuration the fillet supports the build up of a horse-shoe vortex leg, Figure 10 (mid) plane 1. From the displacement created by the fillet a redistribution of the flow occurs: The suction surface horse-shoe vortex leg disappears and a new vortex arises, which turns in the opposite direction, see plane 2 in Figure 10 (mid). This 'fillet'-vortex blocks the cross flow and transports high energy material towards the surface, leading to the relative maximum in Mach number already observed in Figure 8.

5.4. Spanwise flow distributions

Flow Angles Non-dimensional deviation of the pitch averaged flow angles from the 2D flow are presented for the three configurations in Figure 11. At the inlet of the computational domain (about $x/c_{ax} = -2.0$) a constant inlet flow angle is prescribed. At $x/c_{ax} = -0.5$, approximately the position of the trailing edge of a hypothetical upstream blade row, only a weak deviation of the flow angle compared to the 2D flow in the mid section is found for the reference and the bulb configuration.

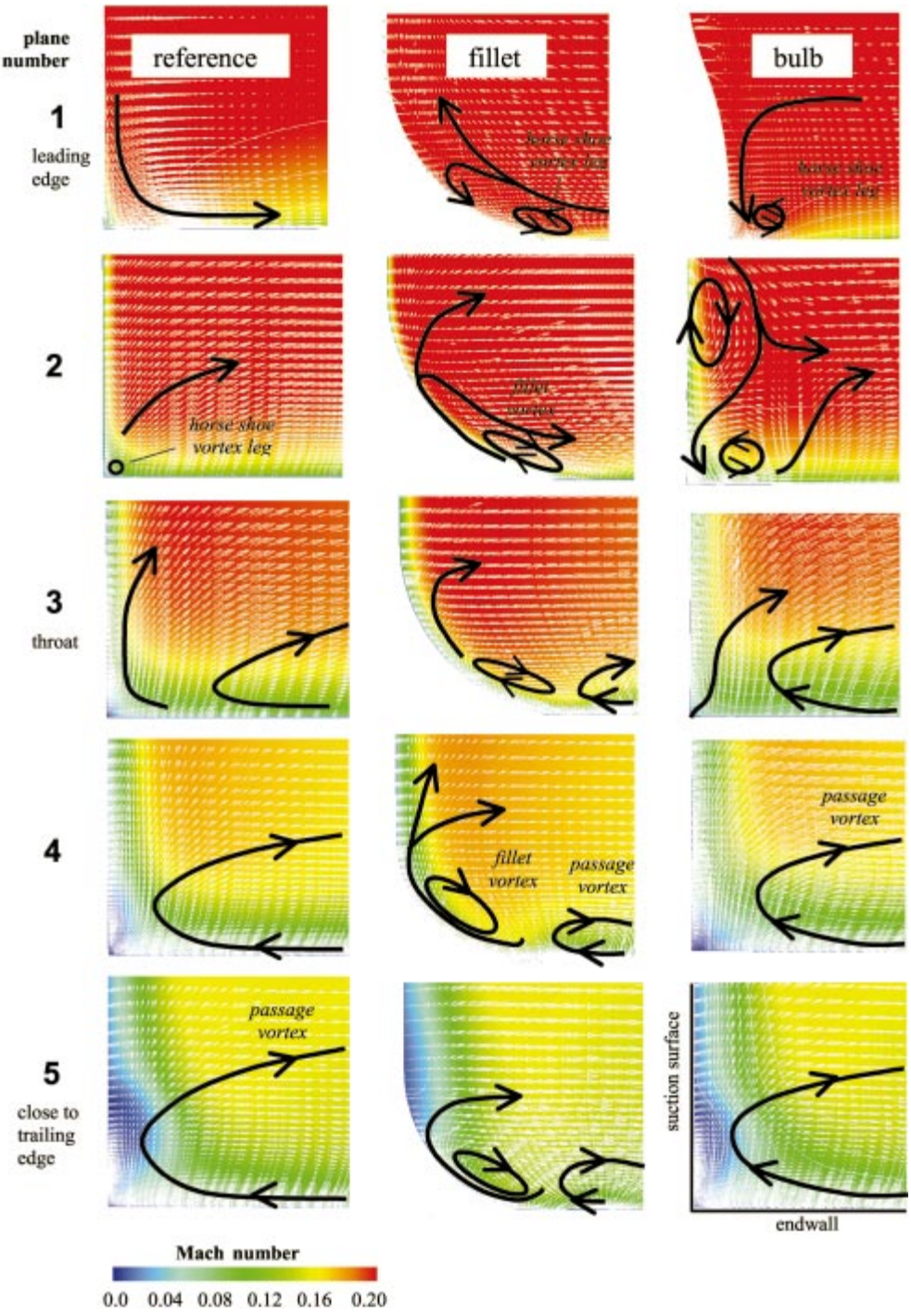

Figure 10. Iso-Mach surfaces and secondary flow vectors in planes normal to suction surface

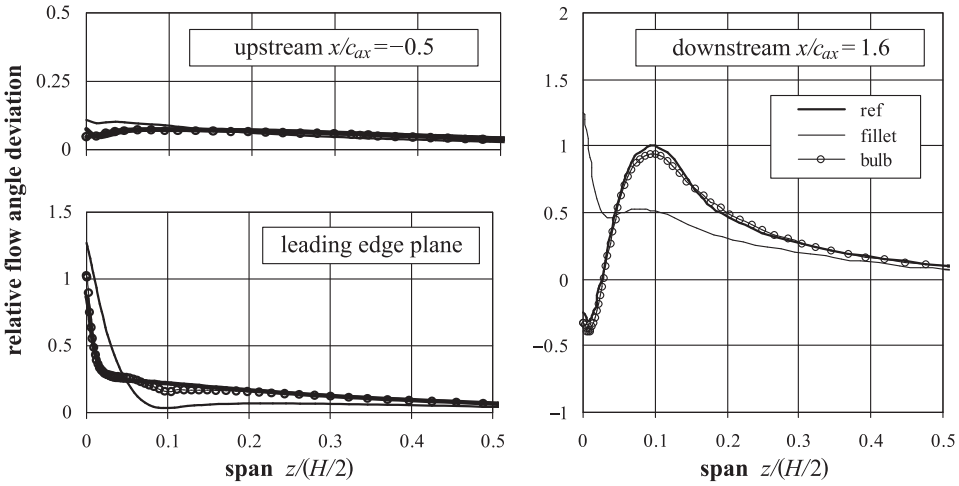

Figure 11. Non-dimensional deviation $\delta\beta/\delta\beta_{\max,\mathrm{ref}}$ of pitch-averaged flow angles for datum design, fillet and bulb configuration

A considerable increase in flow angle is generated by the fillet close to the endwall. This indicates the fillet radius to cause large blade interaction effects. At the leading edge the incidence for the fillet further increases. Downstream of the trailing edge at $x/c_{ax} = 1.6$ the reference blade reveals the typical exit flow angle behaviour with an underturning close to $z/(H/2) = 0.1$ and an overturning at the endwall. A slight reduction in underturning is found for the bulb. Close to the wall the fillet radius causes a considerable reduction in turning. With increasing wall distance the blockage generated by the fillet accelerates the flow in the passage and nearly halves the underturning compared to the reference blade. The large reduction in turning close to the wall for the fillet case is regarded not only to be dependent on the lapse of any Kutta-condition, but on the formulation of the boundary conditions: With the inlet condition in a compressor enforced by the upstream blade row at about $x/c_{ax} = -0.5$, for the cascade simulations the inlet of the computational domain is situated about two axial chord length upstream, which facilitates inlet flow angle changes and promotes higher local incidences.

By adding further results of an 8% chord fillet configuration the impact of the fillet radius on the relative minima and maxima of the exit flow angle deviation is given in Figure 12. An approximately linear dependency of the deviation on the fillet magnitude is found close to the wall, while the magnitude of the underturning at some distance from the wall was nearly independent of the size of the fillet. A comparison of the fillet magnitude in Figure 12 with actual designs indicates the fillet with $R/c = 16\%$ to be slightly beyond the experience range. But with some results for the $R/c = 8\%$ fillet added it is felt well suited to work out vortex structures more clearly.

Losses Compared to the reference case the losses for the fillet configuration were found to increase in the wall region and to decrease at some distance from the endwall with the removal of the separation region. The bulb configuration revealed only a slight decrease in loss at the location of the maximum underturning.

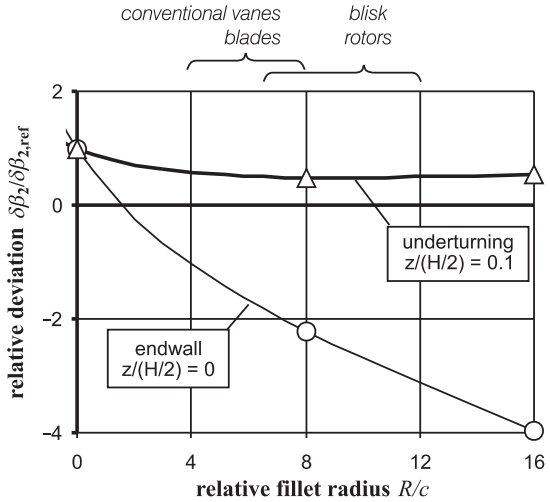

Figure 12. Normalized exit flow angle deviation at $z/(H/2) = 0$ and $z/(H/2) = 0.1$ as function of relative fillet radius

6. Conclusions

A plane compressor cascade was designed to investigate the influence of fillet radii and modified thickness distribution at the hub on secondary flows. High incidences are considered similar to the flow conditions of a compressor blade close to stall, with a confined separation on the suction surface close to the endwall. Numerical investigations are performed with the 3D Navier-Stokes code TRACE_S in the fully turbulent mode applying a standard k-ε turbulence model. The fillet radius configuration with $R/c = 16\%$ revealed a complex vortex system with a so-called 'fillet'-vortex turning in the same sense as the passage vortex. Separation of the boundary layer on the suction surface was removed completely. Compared to the reference configuration the fillet geometry was demonstrated to increase local incidence and decrease turning in the vicinity of the endwall. This, however, indicates blade interaction effects to be generated by real geometry configurations with fillet radii. A special bulb configuration designed at TU Dresden was successfully used to amplify the suction surface leg of the horse-shoe vortex, which rotates in the opposite direction to the passage vortex. By that convective loss transport was blocked and the suction surface separation observed for the reference blade reduced in size.

For the present investigations on a compressor blade in a cascade the following may be stated: Adding a fillet to the blade profile at the endwall does not significantly alter the losses in the vicinity of the endwall but mainly increases blockage and reduces the 3D discharge flow angle changes known as under- and overturning. This result indicates that such real geometry effects should be included in turbomachinery design systems.

Acknowledgements

The support of the optimised compressor blade investigations as part of the AG Turbo II programme is gratefully acknowledged. The authors would also like to thank G. H. Frantz of MTU München GmbH for his support in complex geometry design.

References

[1] Denton J D 1994 *ASME J. Tubomachinery* **113** 621
[2] Debruge L L 1980 *ASME J. Eng. for Power* **102** 984
[3] Curlett B P 1991 *Rep. NASA-TM-105347*
[4] Calvert W J and Ginder R B 1999 *Proc. Instn. Mech. Engrs., Part C, J. Mech. Eng. Science* **213** 419
[5] Breugelmans F A E 1999 *VKI LS 1999-02 on Turbomachinery Blade Design Systems*
[6] Escuret J F, Veysseyre Ph, Villain M, Savarese S, Bois G and Naviere H 1997 *ASME Paper* **97-GT-471**
[7] LeJambre C R, Zacharias R M, Biederman B P, Gleixner A J and Yetka C J 1996 *ASME Paper* **95-GT-343**
[8] Boos P, Möckel H, Henne J M and Selmeier R 1998 *ASME Paper* **98-GT-0432**
[9] Roberts W B, Serovy G K and Sandercock D M 1985 *ASME Paper* **85-GT-189**
[10] Turner M G, Liang T, Beauchamp P P and Jennions I K 1993 *ASME Paper* **93-GT-38**
[11] Sauer H, Müller R and Vogeler K 2000 *ASME Paper* **2000-GT-473**
[12] Fritsch G and Möhres W 1997 *Proc. 9th Parallel CFD Conf.*, Manchester, UK
[13] Fritsch G, Hoeger M, Blaha C and Bauer D 1997 *AIAA Paper* **97-2876**
[14] Hawthorne W R 1955 *J. Mech. Appl. Math.* **8** (3) 266
[15] Came P M and Marsh H 1974 *J. Mech. Eng. Science* **16** 391
[16] Langston L S, Nice M L and Hooper R M 1977 *ASME J. Eng. for Power* **99** 21
[17] Sieverding C H 1984 *ASME Paper* **84-GT-78**
[18] Stark U and Bross S 1996 *85th PEP Symposium*, Derby, UK, *AGARD* CP-571